THE AMERICAN SOCIETY OF MECHANICAL ENGINEERS
Three Park Avenue, New York, N.Y. 10016-5990

99-GT-21

STEADY AND DYNAMIC STALL ANALYSIS OF THE NLR 7301 AIRFOIL

Stefan Weber* **and Max F. Platzer†**
Department of Aeronautics and Astronautics
Naval Postgraduate School
Monterey, California

ABSTRACT

The static and dynamic stall behavior of the supercritical NLR 7301 airfoil is analyzed with a 2D thin-layer Navier-Stokes code. The code solves the compressible Reynolds-averaged Navier-Stokes equations with an upwind biased numerical scheme in combination with the Baldwin-Lomax or the Baldwin-Barth turbulence models. The effect of boundary layer transition is incorporated using the transition length model of Gostelow et al. The transition onset location is determined with Michel's formula or it can be specified as an input parameter. The two turbulence models yield significantly different steady-state lift coefficients at incidences greater than 8 degrees. Also, the lift hysteresis loops are strongly affected by the choice of the turbulence model. The use of the one-equation Baldwin-Barth model together with the Gostelow transition model is found to give substantially better agreement with the experimental data of McCroskey et al. than the Baldwin-Lomax model.

NOMENCLATURE

a_∞	free stream speed of sound
c	chord length
c_l	lift coefficient
c_p	pressure coefficient
$c_{\epsilon_1}, c_{\epsilon_2}$	constants of turbulence model
e	total energy per unit volume
f	frequency in Hertz
f_2	damping function
k	reduced frequency, $2\pi fc/U_\infty$
M_∞	free stream Mach number
N	non-dimensional breakdown rate parameter
n	spot generation rate
P	turbulence production term
q_t	free-stream turbulence at x_t [%]
Re	Reynolds number cU/ν
R_T	turbulent Reynolds number, $k^2/\nu\dot{\epsilon}$
t	nondimensional time, $\tilde{t}a_\infty/c$
U	local free-stream velocity
U_∞	free stream velocity magnitude
u, v	velocity components
x	coordinate parallel to chord
x_t	transition onset location
$\dot{x}\|_{wall}$	velocity component of blade surface
$\dot{y}\|_{wall}$	velocity component of blade surface
y^+	nondimensional normal wall distance
α	spot spreading half angle, angle of attack
γ	intermittency factor
κ	ratio of specific heats
λ_θ	pressure gradient parameter, $(\theta^2/\nu)/(dU/dx)$
λ_{θ_t}	pressure gradient parameter at x_t
μ	viscosity
ν	kinematic viscosity
ν_t	turbulent viscosity
θ	boundary layer momentum thickness
ρ	density
ρ_∞	free stream density
σ	spot propagation parameter
σ_ϵ	constant of turbulence model
$\dot{()}$	differentiation with respect to t
$\|_{wall}$	quantity on the surface of the blade

* Post Doctoral Researcher, Deutsche Forschungsgemeinschaft (DFG)

† Professor of Aeronautics and Astronautics, Fellow ASME

Presented at the International Gas Turbine & Aeroengine Congress & Exhibition
Indianapolis, Indiana — June 7–June 10, 1999

INTRODUCTION

Carta and Lorber (1987) published experimental data which showed that small amplitude oscillations of propeller blades near stall may be quite unstable. Stall flutter has also been encountered on fan and compressor blades of jet engines operating in part-speed conditions at high angles of attack, as discussed for example by Sisto (1987). Unfortunately, the prevention of stall flutter of propeller and turbomachinery blades is still heavily dependent on semi-empirical information which makes it difficult to assure the flutter safety of newly designed blades where few test data are available. The very complex unsteady flow phenomena which occur in these propeller and compressor operating conditions greatly impede the development of non-empirical prediction methods. Nevertheless, recent progress in the numerical analysis of dynamic stall phenomena, as summarized by Ekaterinaris and Platzer (1997), suggests the possibility of developing prediction methods which are based on solutions of the viscous flow equations.

The present paper is a continuation of systematic studies begun by Ekaterinaris and Platzer (1995, 1996) and Sanz and Platzer (1998) to explore the feasibility of computing stall onset and stall flutter using the Navier-Stokes equations in combination with advanced turbulence and transition models. Encouraging results were obtained for the NACA 0012 and Sikorsky SC 1095 airfoils. It is the objective of the present paper to report similar computations for the NLR 7301 airfoil. This airfoil was chosen for the study because detailed experimental data are available from McCroskey et al. (1982) and Schewe and Deyhle (1996). Single airfoil computations are of immediate interest for propeller and propfan applications. For example, Ducharme and Crawley (1987) showed that the mass ratio of an unducted fan is much closer to values of an isolated wing than of turbofans. Furthermore, stall flutter is a highly nonlinear phenomenon (Dowell et al., 1978) making it advisable to explore the ability of modern CFD methods to predict the unsteady flow separation and re-attachment behavior. Work is currently in progress to extend this approach to stall flutter of turbomachinery cascades.

NUMERICAL METHOD

The unsteady, nonlinear, compressible Navier-Stokes algorithm solves the strong conservation-law form of the two-dimensional, thin-layer Navier-Stokes equations in a curvilinear coordinate system (ξ, η). The governing equations are given in vector form by:

$$\partial_t \hat{\mathbf{Q}} + \partial_\xi \hat{\mathbf{E}} + \partial_\eta \hat{\mathbf{F}} = Re^{-1} \partial_\eta \hat{\mathbf{S}} \tag{1}$$

where $\hat{\mathbf{Q}}$ is the vector of conservative variables

$$\hat{\mathbf{Q}} = \frac{1}{J} \begin{Bmatrix} \rho \\ \rho u \\ \rho v \\ e \end{Bmatrix}, \tag{2}$$

$\hat{\mathbf{E}}$ and $\hat{\mathbf{F}}$ are the inviscid flux vectors

$$\hat{\mathbf{E}} = \frac{1}{J} \begin{Bmatrix} \rho U \\ \rho u U + \xi_x p \\ \rho v U + \xi_y p \\ (e+p)U - \xi_t p \end{Bmatrix}, \tag{3}$$

$$\hat{\mathbf{F}} = \frac{1}{J} \begin{Bmatrix} \rho V \\ \rho u V + \eta_x p \\ \rho v V + \eta_y p \\ (e+p)V - \eta_t p \end{Bmatrix} \tag{4}$$

and $\hat{\mathbf{S}}$ is the thin-layer approximation of the viscous fluxes in the η direction (normal to the airfoil surface)

$$\hat{\mathbf{S}} = \frac{1}{J} \begin{Bmatrix} 0 \\ \mu m_1 u_\eta + (\mu/3) m_2 \eta_x \\ \mu m_1 v_\eta + (\mu/3) m_2 \eta_y \\ \mu m_1 m_3 + (\mu/3) m_2 m_4 \end{Bmatrix}, \tag{5}$$

where

$$m_1 = \eta_x^2 + \eta_y^2, \tag{6}$$

$$m_2 = \eta_x u_\eta + \eta_y v_\eta, \tag{7}$$

$$m_3 = (u^2 + v^2)/2 + (\kappa - 1)^{-1} Pr^{-1} \partial_\eta (a^2), \tag{8}$$

and

$$m_4 = \eta_x u + \eta_y v. \tag{9}$$

The terms U and V are the contravariant velocity components given by:

$$U = u\xi_x + v\xi_y + \xi_t \tag{10}$$

and

$$V = u\eta_x + v\eta_y + \eta_t \tag{11}$$

and J is the metric Jacobian, where

$$J^{-1} = x_\xi y_\eta - x_\eta y_\xi \ . \tag{12}$$

Pressure is related to the other variables through the equation of state for an ideal gas:

$$p = (\kappa - 1)\left[e - \rho(u^2 + v^2)/2\right] \ . \tag{13}$$

Eqs. (1-13) are nondimensionalized using c as the reference length, a_∞ as the reference velocity, c/a_∞ as the reference time, ρ_∞ as the reference density and $\rho_\infty a_\infty^2$ as the reference energy. The form of the equations does not change because of the nondimensionalization.

For Euler solutions the viscous terms on the RHS are set to zero, and flow tangency boundary conditions are applied at the surface. For Navier-Stokes solutions the no-slip condition is applied at the surface. Density and pressure are extrapolated to the surface for both Euler and Navier-Stokes

solutions. For unsteady motions the flow-tangency and no-slip conditions are modified to include the local motion of the surface which also contributes to the pressure on the surface. Therefore, the momentum equation normal to the surface (η direction) is solved to predict the pressure for a viscous flow more accurately:

$$\partial_\eta p|_{wall} = -\frac{1}{\nabla^2 \eta}\left[\rho\, \partial_t \left\{ \begin{array}{c} \dot{x}|_{wall} \\ \dot{y}|_{wall} \end{array} \right\} \cdot \nabla\eta + \partial_\eta p|_{wall} \nabla\xi \cdot \nabla\eta\right] . \quad (14)$$

where $\dot{x}|_{wall}$ and $\dot{y}|_{wall}$ are the components of the blade velocity. Furthermore, it is assumed that the grid is orthogonal at the surface, and therefore $\nabla\xi \cdot \nabla\eta = 0$. If the blade does not move, the normal pressure gradient is equal to zero according to boundary layer theory.

The time-integration is performed using the third order upwind biased, factorized, iterative, implicit scheme of Chakravarthy and Osher (1985) tested by Ekaterinaris and Platzer (1996) and given by:

$$\begin{aligned} &\left[I + h_\xi\left(\nabla_\xi \hat{A}^+_{i,k} + \Delta_\xi \hat{A}^-_{i,k}\right)\right]^p \\ &\times \left[I + h_\eta\left(\nabla_\eta \hat{B}^+_{i,k} + \Delta_\eta \hat{B}^-_{i,k} - Re^{-1}\delta_\eta \hat{M}_{i,k}\right)\right]^p \\ &\times \left(\hat{Q}^{p+1}_{i,k} - \hat{Q}^p_{i,k}\right) \\ &= -\left[\left(\hat{Q}^p_{i,k} - \hat{Q}^n_{i,k}\right)\right. \\ &\quad + h_\xi\left(\hat{E}^p_{i+1/2,k} - \hat{E}^p_{i-1/2,k}\right) \\ &\quad + h_\eta\left(\hat{F}^p_{i,k+1/2} - \hat{F}^p_{i,k-1/2}\right) \\ &\quad \left. - Re^{-1}h_\eta\left(\hat{S}^p_{i,k+1/2} - \hat{S}^p_{i,k-1/2}\right)\right] . \end{aligned} \quad (15)$$

In Eq. (15), $h_\xi = \Delta t/\Delta\xi$ etc., $\hat{A}^\pm = \partial\hat{E}/\partial\hat{Q}$ etc. are the flux Jacobian matrices and ∇, Δ and δ are the forward, backward and central difference operators, respectively. The quantities $\hat{E}_{i+1/2,k}$, $\hat{F}_{i,k+1/2}$ and $\hat{S}_{i,k+1/2}$ are numerical fluxes. The superscript $(\cdot)^n$ denotes the time step, and the superscript $(\cdot)^p$ refers to Newton subiterations within each time step. The inviscid fluxes, $\hat{E}$ and $\hat{F}$, are evaluated using Osher's third-order upwinding scheme (Rai and Chakravarthy, 1988). For the linearization of the left-hand side of Eq. (15) the flux Jacobian matrices, A and B, are evaluated by the Steger-Warming flux-vector splitting (Steger and Warming, 1981). The viscous fluxes are computed with second-order central differences. Time accuracy is improved by performing Newton subiterations to convergence at each step. These subiterations minimize the linearization and factorization errors and help drive the left-hand side of Eq. (15) to zero at each time step. The present authors found that larger CFL numbers (i.e., a larger time step) could be used if the number of Newton iterations was increased. The optimum seemed to depend on the grid topology and flow conditions, but the best computational performance seemed to occur with 2 to 3 sub-iterations for Navier-Stokes simulations. The Navier-Stokes solver has been tested extensively in a variety of unsteady subsonic and transonic studies, such as Clarkson et al. (1993), Grohsmeyer et al. (1991), Ekaterinaris et al. (1994), and Ekaterinaris and Platzer (1996).

TURBULENCE MODELING

The turbulence modeling is based either on the standard zero equation model of Baldwin and Lomax (1978) or the one equation model of Baldwin and Barth (1990).

Originally, the Baldwin-Barth turbulence model was derived from the $k-\epsilon$ model by introducing some simplifying assumptions. It does not need evaluation of ambiguous length scales like the algebraic model by Baldwin and Lomax does, and it describes the physics of the turbulent flow more accurately. It requires the numerical solution of the following partial differential equation for a modified turbulent Reynolds number $\nu\tilde{R}_T$:

$$\begin{aligned} \frac{D(\nu\tilde{R}_T)}{Dt} &= (c_{t_2}f_2 - c_{t_1})\sqrt{\nu\tilde{R}_T P} \\ &\quad + (\nu + \frac{\nu_t}{\sigma_\epsilon})\nabla^2(\nu\tilde{R}_T) - \frac{1}{\sigma_\epsilon}(\nabla\nu_t)\cdot\nabla(\nu\tilde{R}_T) . \end{aligned} \quad (16)$$

The field quantity $\tilde{R}_T$ is related to the $k-\epsilon$ quantities by $R_T = k^2/\nu\epsilon = \tilde{R}_T f_3(\tilde{R}_T)$, where $f_3(\tilde{R}_T)$ is a damping function, which depends on the wall distance. All the terms and constants are evaluated according to Baldwin and Barth (1990). The solution of this equation is performed using an implicit factored ADI solver and is decoupled from the mean-flow equations. At the inflow boundary a free-stream turbulent Reynolds number of 0.1 was chosen. The implementation of the Baldwin and Barth turbulence model to the code was previously tested and published by Ekaterinaris and Platzer (1996) and Sanz and Platzer (1998).

TRANSITION MODELING

The transition modeling for both turbulence models follows Sanz and Platzer (1998). In this publication the model of Gostelow et al. (1996) was introduced which permits the calculation of the transition length as a function of pressure gradient and free-stream turbulence level. This method continuously adjusts the turbulent spot growth in response to changes in the local pressure gradient.

The intermittency distribution in the transitional region is given by:

$$\gamma(x) = 1 - exp\left[-n\int_{x_t}^{x_i}\frac{\sigma}{tan\alpha}\left(\frac{dx}{U}\right)\int_{x_t}^{x_i} tan\alpha dx\right] , \quad (17)$$

where the correlations for the variation of σ and α as functions of the pressure gradient parameter λ_θ are

$$\alpha = 4 + (22.14/(0.79 + 2.72exp(47.63\lambda_\theta))) , \quad (18)$$

$$\sigma = 0.03 + (0.37/(0.48 + 3.0exp(52.9\lambda_\theta))) \; . \qquad (19)$$

The spot generation rate n is inferred from the dimensionless breakdown rate parameter N:

$$N = n\sigma\lambda_{\theta_t}^3/\nu, \qquad (20)$$

$$N = 0.86 \times 10^{-3} exp(2.134\lambda_{\theta_t} ln(q_t) \qquad (21)$$
$$- 59.23\lambda_{\theta_t} - 0.564ln(q_t)), \; for \; \lambda_{\theta_t} \leq 0 \; .$$

$$N = N(\lambda_\theta = 0) \times exp(-10\sqrt{\lambda_{\theta_t}}), \quad for \; \lambda_{\theta_t} > 0 \; . \qquad (22)$$

The above formulas imply a maximum value for σ and α for high negative values, but the spot generation rate is allowed to increase to infinity for high negative values of λ_{θ_t}. The value of the intermittency $\gamma(x)$ is zero for $x \leq x_{t_i}$ and increases downstream from the transition point exponentially to a maximum value of one, which corresponds to fully-turbulent flow. An effective eddy viscosity for the transitional region is obtained by scaling the turbulent eddy viscosity computed from the mean flow by $\gamma(x)$, i.e. $\mu_{trans} = \gamma(x)\mu_{turb}$.

Sanz and Platzer (1998) have used the Gostelow model which was originally developed for attached flow for the prediction of laminar separation bubbles by using the spot generation rate as a second adjustable parameter besides the location of transition onset. They investigated the influence of the spot generation rate on the separation bubble by either limiting the breakdown rate parameter to one which forces instantaneous transition or by assuming the value for a zero pressure gradient.

In the present study the breakdown rate parameter was chosen to force instantaneous transition for all computations and the transition onset was either predicted by the Michel criterion (Cebeci and Bradshaw, 1977) or by specification as an input parameter.

RESULTS AND DISCUSSION

All steady state and unsteady computations for the NLR 7301 airfoil were performed on a C-type Navier-Stokes grid with 221×91 grid points. The initial wall spacing used was 2×10^{-5} resulting in a $y^+ < 3$ for the chosen Mach number of 0.3 and the Reynolds number of 4×10^6. 40 grid points were used in the wake and the farfield boundary extended 20 chord lengths from the surface. The grid is shown in Fig. 1.

A detailed set of measurements for the steady flow at different angles of attack, Mach numbers up to 0.3 and Reynolds numbers up to 4×10^6 have been performed at the NASA Ames Research Center by McCroskey et al. (1982). They investigated the static and dynamic characteristics of seven helicopter blades and a supercritical fixed wing airfoil. The supercritical airfoil was chosen for the present study because it is and will be experimentally investigated at the DLR Goettingen to determine its flutter behaviour.

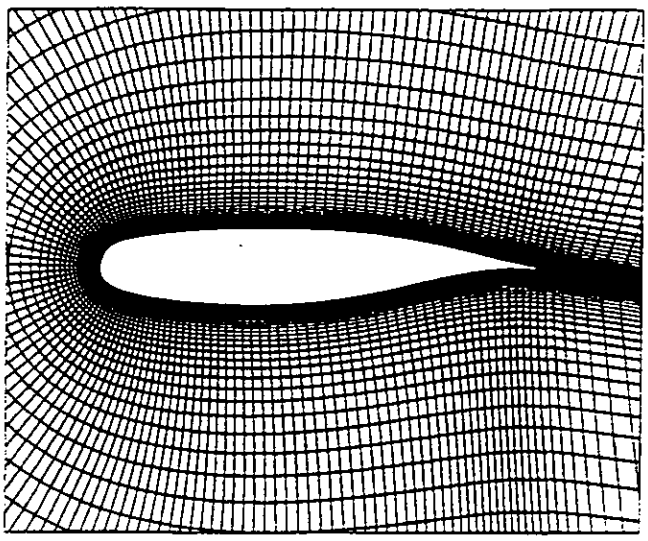

FIG. 1 C-type grid for the NLR 7301 airfoil

Fully Turbulent Steady-State Computations

The steady state computations as well as the measurements were obtained at fixed angles of attack in a range from -5 degrees up to 20 degrees. The Mach number for the experiments was approximately 0.3 and the Reynolds number 4×10^6. In Fig. 2 the computed steady-state results are compared with the measured data.

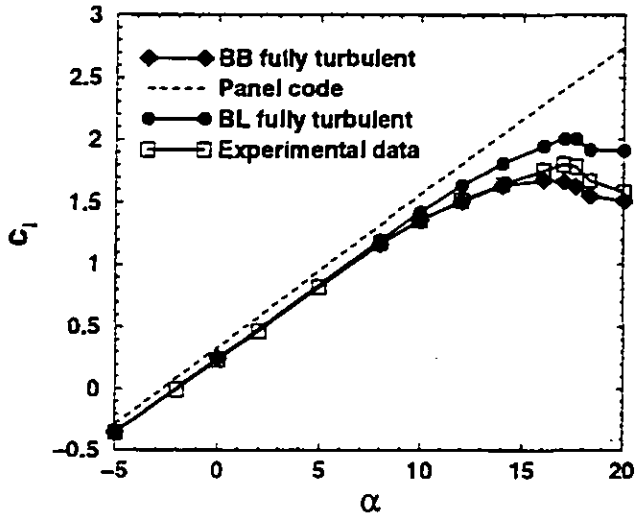

FIG. 2 Lift coefficient versus angle of attack, experimental data by McCroskey et al.

Fig. 2 shows the linear results obtained with the potential flow panel code UPOT (Teng, 1987) and results for viscous computations using the Baldwin-Lomax (BL) and the Baldwin-Barth (BB) turbulence model. All viscous computations were performed assuming fully turbulent flow. The BL and BB computed lift coefficients are in close agreement with the measured data for a range of the angle of attack

of -5 degrees to 8 degrees. Although the BL and BB computed lift coefficients are almost the same up to α= 8 degrees, simulations with BB show more flow separation near the trailing edge on the upper surface than BL. For both models this separation grows significantly with increasing angle of attack but the flow stays attached longer for flow simulations with BL due to BL computing higher viscosity. The locations of the separation onset s/c versus the angle of attack for both turbulence models can be seen in Fig. 3. Once the flow is separated, it does not re-attach. For flow angles of 0 and 5 degrees both turbulence models show no separation.

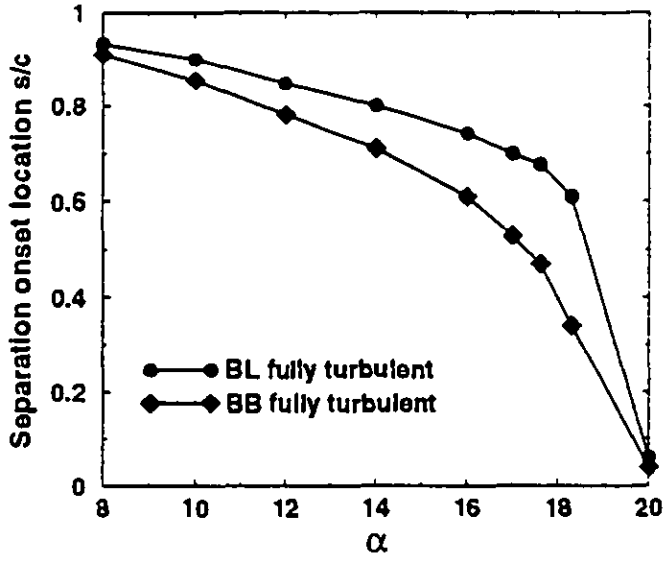

FIG. 3 Variation of the separation onset location

Steady-state solutions in terms of the pressure coefficient distributions versus the chord for α = 14, 17 and 17.6 degrees are given in Figs. 4 to 6.

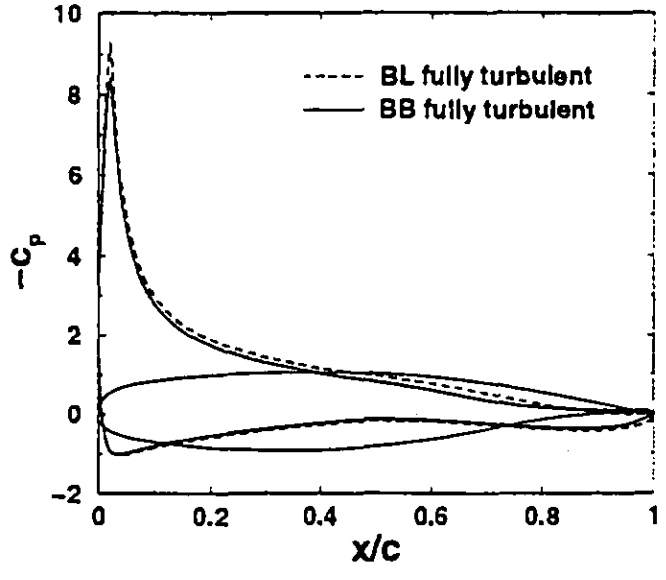

FIG. 4 Pressure coefficient versus chord for α = 14 degrees

These plots show that a higher suction peak is predicted by BL than by BB. Furthermore, the BB model yields a much more constant static pressure in the separation region, as can be seen from the pressure plateaus in front of the trailing edge. Both models predict a nonlinear increase of the lift coefficient for angles of attack higher than 8 degrees. The lift coefficients calculated with the BB model are in good agreement with the measurements up to 14 degrees while the BL model overpredicts the lift for angles of attack in excess of 8 degrees due to the higher suction peak and smaller flow separation.

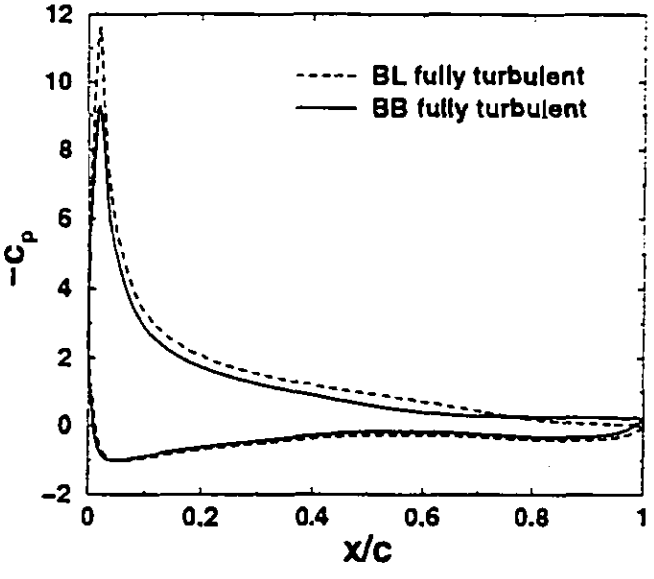

FIG. 5 Pressure coefficient versus chord for α = 17 degrees

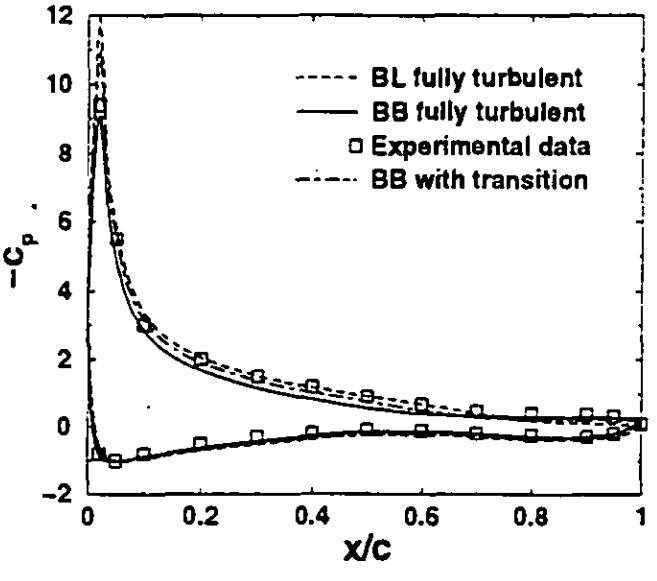

FIG. 6 Pressure coefficient versus chord for α = 17.6 degrees, experimental data by McCroskey et al.

The BL model predicts the highest lift coefficient at 17 degrees angle of attack in agreement with the experiments, but overpredicts the lift coefficient by 11%. BB predicts the highest lift at an angle of attack of 16 degrees. For angles of attack greater than 14 degrees, the BB model yields a lower lift coefficient than the measurements. It underpredicts the lift by 8%. For angles of attack greater than 17 degrees the convergence behaviour of both models is quite different. Although the flow, after reaching the stall angle of approximately 17 degrees, will no longer be steady and therefore the measured and the computed data have to be regarded as averaged values, the BL model converges to a constant lift coefficient up to an angle of attack of 17.6 degrees. In Fig. 6 the BL and BB computed pressure distributions are compared with the experimental data.

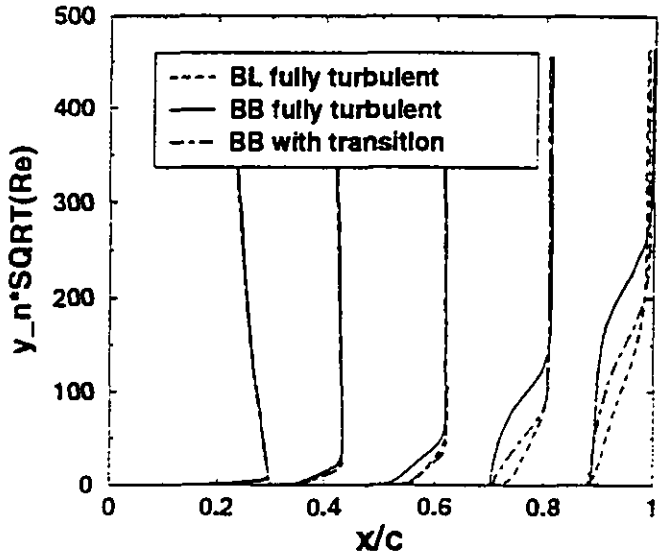

FIG. 7 Boundary layer profiles for $\alpha = 17.6$ degrees

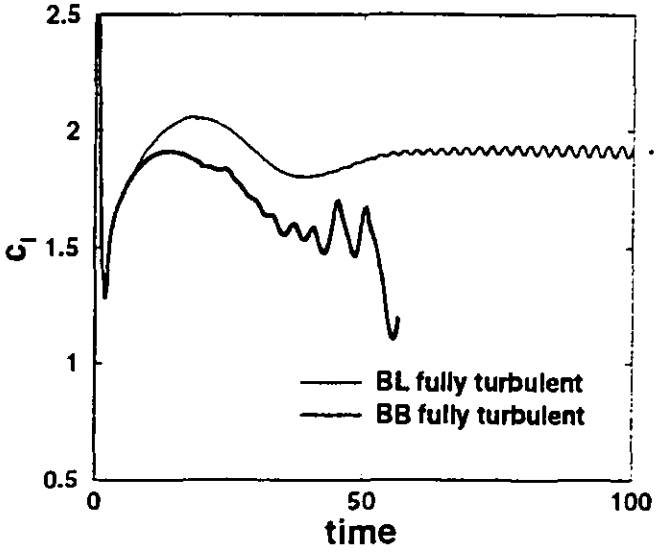

FIG. 8 Time development of the lift coefficient for $\alpha = 20$ degrees

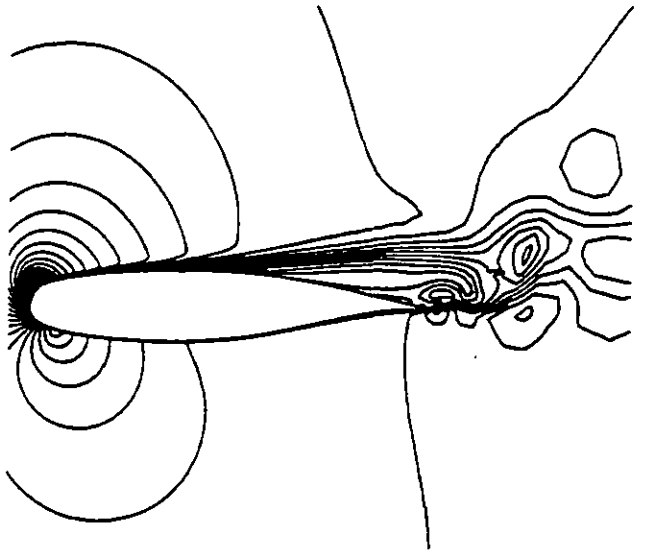

FIG. 9 Instantaneous Mach number distribution for $\alpha = 20$ degrees computed with the BL model

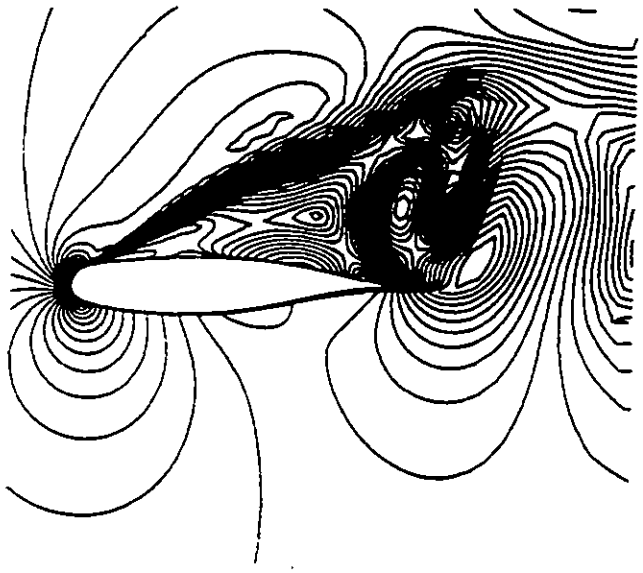

FIG. 10 Instantaneous Mach number distribution for $\alpha = 20$ degrees computed with the BB model

It can be seen that the BB computed flow on the pressure side is in slightly better agreement with the experiment. On the suction side, except near the suction peak, the BL computed pressures agree with the experiment up to 70% chord. Further downstream the pressure is too low. The BB computed suction peak almost yields the measured peak, but the pressure coefficient between 10% and 70% chord is underpredicted which explains the underprediction of the lift coefficient (Fig. 2). The development of the boundary layer along the airfoil for 17.6 degrees is given in Fig. 7. For flow angles exceeding 17.6 degrees the computed lift coefficients are no longer steady. This can be seen in Fig. 8 where

the BL and the BB computed lift histories are plotted for the case of 20 degrees incidence angle. It is shown that the BL computed lift is periodic but reaches values which are considerably higher than the measured value. The BB computed lift, on the other hand, approaches values considerably closer to the measured value, but then drops dramatically. Figs. 9 and 10 depict typical time-instantaneous flow fields computed with the BL and the BB models. The BB model is seen to produce massively separated flow. It should be noted that all the computations were performed time-accurately.

Steady-State Computations with Transition

The fully turbulent flow computations described in the previous section show that the BB model is superior to the BL model. However, the sensitivity to transitional flow effects is an important aspect which needs to be studied. Therefore, the computations were repeated with the BB model by assuming that transition starts at $x/c = 0.02$ for angles of attack between 14 and 17.6 degrees. The numerical results can be seen in Fig. 11.

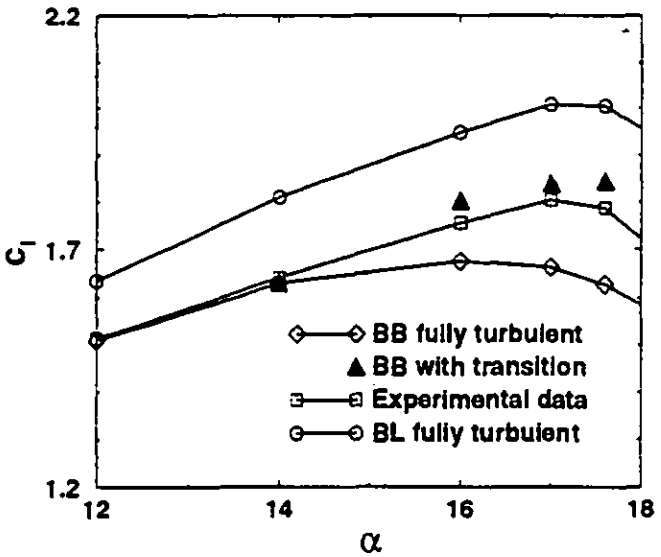

FIG. 11 Lift coefficient versus angle of attack, experimental data by McCroskey et al.

Fig. 11 shows that transition becomes important as the incidence angle is increased. Incorporation of transition substantially improves the agreement with the measured lift values in the high angle of attack range. This improvement can also be seen in Fig. 6. On the pressure side the computations with and without transition differ only slightly, but inclusion of transition yields better agreement with the experimental data on the suction side. Only the suction peak is overpredicted. The development of the boundary layer including transition is given in Fig. 7. The separation onset on the suction side was moved downstream from 48% chord without transition to 60% chord with transition.

These numerical results for the NLR 7301 airfoil confirm the findings of Ekaterinaris and Platzer (1996) and Sanz and Platzer (1998) for the NACA 0012 and the Sikorsky SC 1095 airfoils which showed that the numerical prediction of the stall onset is significantly improved by the incorporation of boundary layer transition.

Dynamic Stall Computations

Unsteady computations were performed for the NLR 7301 airfoil oscillating in the pitching mode described by the equation $\alpha(t) = \alpha_o + \alpha_1 \sin\omega t$. As in the experiment, the pitch axis was located at the quarter chord point. Two test cases were considered and compared with the unsteady experimental data.

The first test case had a mean angle of $\alpha_o = 11.96$ degrees and an amplitude of $\alpha_1 = 2.0$ degrees. The reduced frequency was $k = 0.4$, the Mach number 0.293 and the Reynolds number 3.72×10^6. All unsteady numerical computations were performed time accurately after calculating a steady state solution for the mean angle. The unsteady solutions were assumed to be converged if consecutive hysteresis loops did not change. The computations were converged after 3 to 4 periods.

The experiment was performed with free transition. Fig. 12 shows the computed hysteresis loops using the BL model with and without transition.

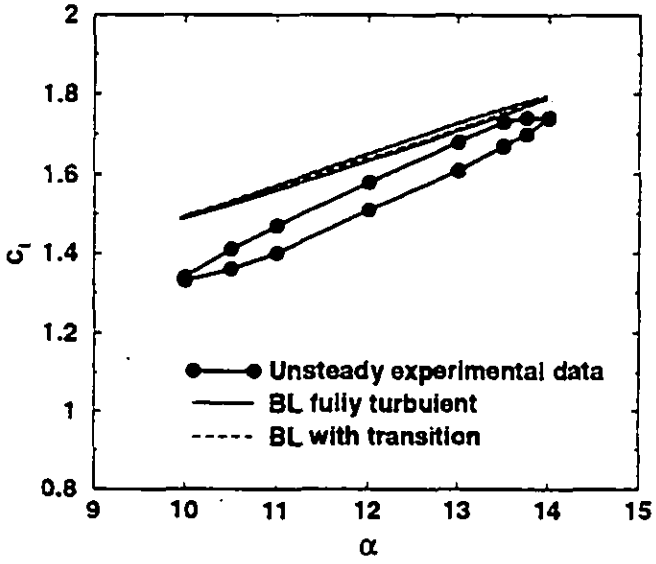

FIG. 12 Unsteady lift coefficient versus angle of attack obtained with the BL model, experimental data by McCroskey et al.

The prediction of the unsteady onset location of transition was obtained with the Michel criterion. It is apparent that the BL model fails to predict the measured hysteresis loop. Repeating the calculations with the BB model, with and without transition, yields much better agreement with the measured hysteresis loop, Fig. 13. Because the unsteady onset locations of transition were not measured, the Michel criterion was used for the calculations.

Additionally, the BB computed unsteady pressure coefficient distributions on the suction side including transition are compared with the measured pressure distributions in Fig. 14 for 20 different angles of attack during the oscillation of the airfoil. It is seen that the computed pressures agree well with the measured distributions.

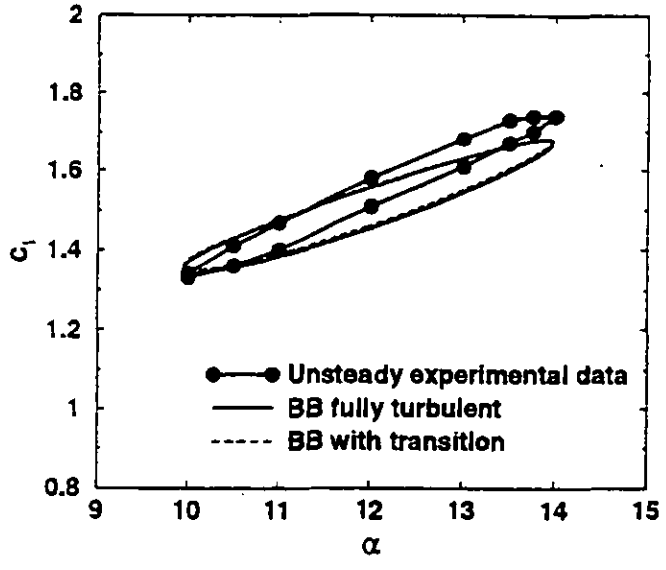

FIG. 13 Unsteady lift coefficient versus angle of attack obtained with the BB model, experimental data by McCroskey et al.

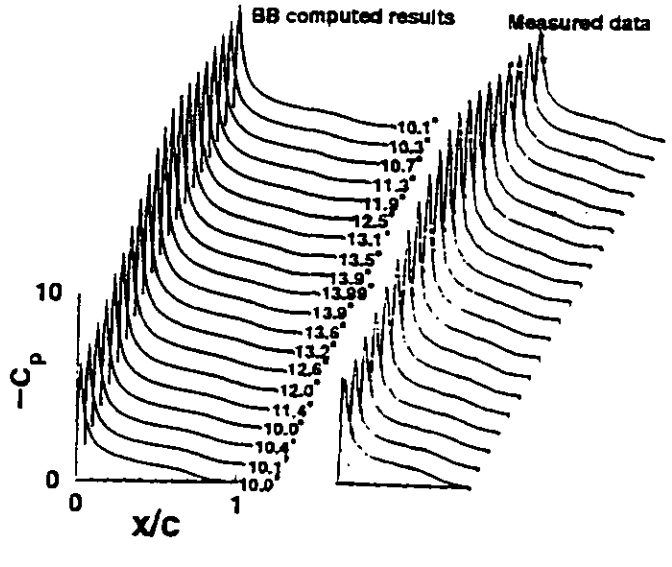

FIG. 14 BB computed unsteady pressure coefficient including transition versus chord in comparison with the measurements by McCroskey et al.

A second series of computations was performed for the case $\alpha_0 = 9.98$ degrees and $\alpha_1 = 4.9$ degrees. The reduced frequency was $k = 0.098$, the Mach number 0.299 and the Reynolds number 3.79×10^6. In Figs. 15 and 16 one can see the numerical results including transition for both turbulence models and the comparison with the experimental data. The unsteady onset locations of transition for both calculations were predicted with Michel's criterion because of the unavailability of relevant experimental transition data.

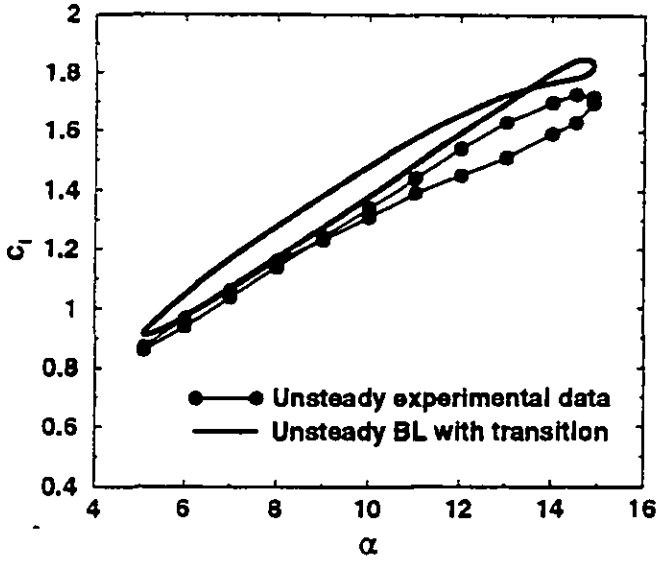

FIG. 15 Unsteady lift coefficient with transition versus angle of attack obtained with the BL model, experimental data by McCroskey et al.

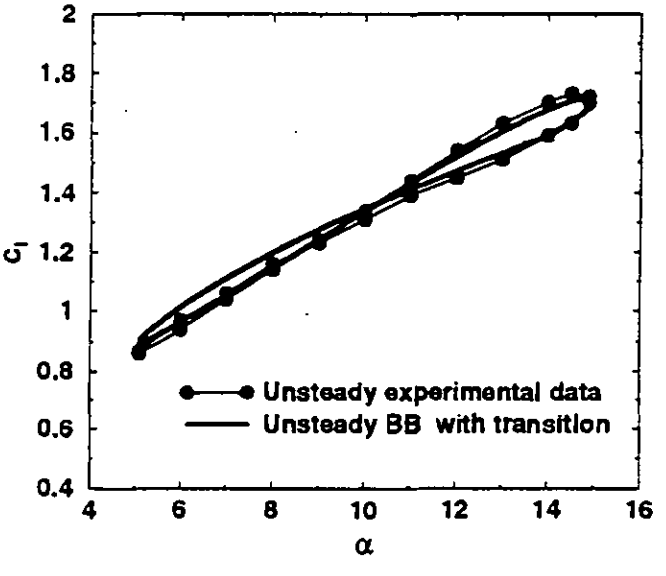

FIG. 16 Unsteady lift coefficient with transition versus angle of attack obtained with the BB model, experimental data by McCroskey et al.

Again, the BB model predicts the measured hysteresis loop much better than the BL model. This is confirmed by the comparison of the computed and measured pressure distributions shown in Fig. 17. The experimental data plotted

in Figs. 15, 16 and 17 were obtained with free transition. A dramatically different hysteresis loop was measured if transition was forced. This is shown in Fig. 18. Unfortunately, no information is available on the precise location of the transition strip. The computation assuming fully turbulent flow is shown in Figs. 17 and 18. Clearly, the inclusion of transition has a negligible influence if transition onset is predicted from Michel's criterion.

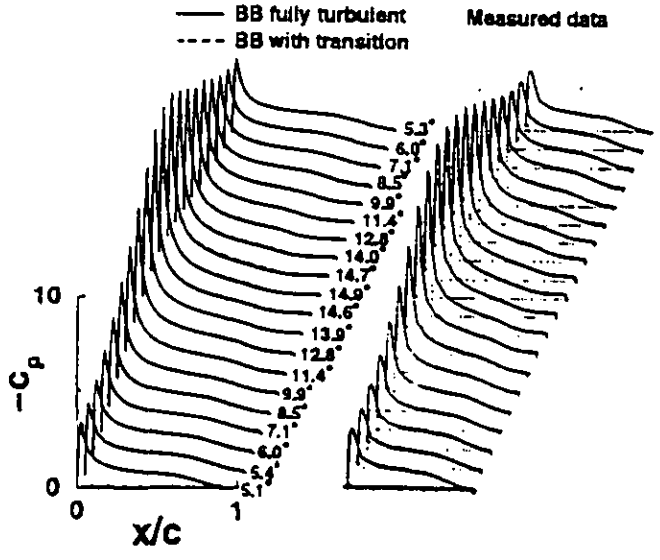

FIG. 17 BB computed unsteady pressure coefficient versus chord in comparison with the measurements by McCroskey et al.

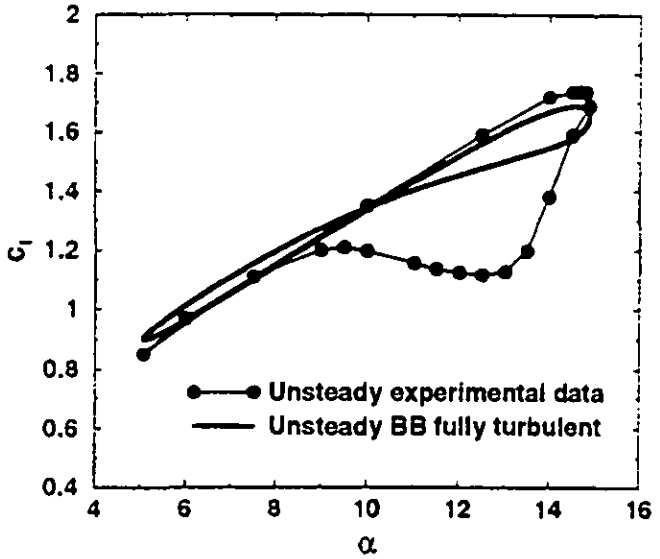

FIG. 18 Fully turbulent unsteady lift coefficient versus angle of attack obtained with the BB model, experimental data by McCroskey et al. for forced turbulent flow

Therefore, it is not surprising that such a computation fails to reproduce the experimental loop of Fig. 18. It is apparent from the measured pressure distributions shown in Fig. 19 that severe flow separation occurs at the start of the downstroke. One would expect that this flow behavior is caused by the sudden burst of a laminar separation bubble. Van Dyken et al. (1996) were able to compute the formation and bursting of the bubble on a NACA 0012 airfoil. Therefore, a computation was performed varying the transition onset location periodically such that the mean position was at $x/c = 0.02$ and the amplitude was 1% of the mean position.

However, this simple attempt to model the flow physics was unsuccessful. Clearly, a more detailed analysis is necessary to clarify the flow mechanism which produces the measured loop.

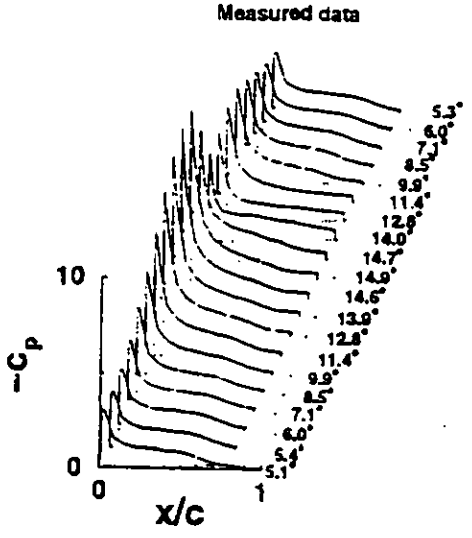

FIG. 19 Unsteady pressure coefficient versus chord for forced fully turbulent flow measured by McCroskey et al.

The average computational effort on steady and unsteady calculations can be summarized as follows:
The steady state computations were performed on SGI Octane workstations. Typical steady state time-accurate computations using the Baldwin-Barth turbulence model including transition needed between 10000 and 25000 time steps in the stall region. The time-accurate unsteady computations were run on a C-90 and a T-932 where between 10000 and 20000 time steps per cycle with 3 Newton subiterations for every time step were necessary.

CONCLUDING REMARKS

A 2D thin-layer Navier-Stokes code was used in conjunction with the Baldwin-Lomax and Baldwin-Barth turbulence models to predict the steady and dynamic stall behavior of the supercritical NLR 7301 airfoil. The influence of transition was investigated by the incorporation of the transition model of Gostelow et al.

The BB model was found to give consistently better agreement with the experimental data than the BL model. Fur-

thermore, the incorporation of boundary layer transition yielded additional improvements, especially for the steady-state analysis, provided that the 'correct' transition onset location was chosen. Further work is clearly needed to develop reliable criteria for transition onset under unsteady adverse pressure gradient conditions. Ultimately, the computations need to be extended to account for 3D effects based on the full Navier-Stokes equations.

ACKNOWLEDGMENT

The first author gratefully acknowledges the support of the Deutsche Forschungsgemeinschaft (DFG) and the Naval Postgraduate School. Also, the authors are indebted to Dr. J. Ekaterinaris, Senior Research Scientist at NIELSEN Engineering and Research Inc., Dr. W. Sanz at the Technical University Graz, Austria and Dr. K. Jones at the Naval Postgraduate School for their advice. NAVO provided computing time on the DoD High Performance Computing Systems.

REFERENCES

Baldwin, B.S. and Lomax.H., 1978, "Thin Layer Approximation and Algebraic Model for Separated Turbulent Flow," AIAA Paper 78-257

Baldwin, B.S., and Barth, T.J., 1990, "A One-Equation Turbulence Transport Model for High Reynolds Number Wall-Bounded Flows," NASA TM 102847

Carta, F.O. and Lorber, P.F., 1987, "Experimental Study of the Aerodynamics of Incipient Torsional Stall Flutter," Journal of Propulsion, Vol 3, No. 2, pp. 164 -170

Cebeci, T. and Bradshaw, 1977, "Momentum Transfer in Boundary Layers," Hemisphere Publishing Corporation, Washington, p. 153

Chakravarthy, S.R. and Osher, S., 1985, "A New Class of High Accuracy TVD Schemes for Hyperbolic Conservation Laws," AIAA Paper 85-0363

Clarkson, J.D., Ekaterinaris, J.A. and Platzer, M.F., 1993, "Computational Investigation of Airfoil Stall Flutter," Proceedings International Symposium on Unsteady Aerodynamics, Aeroacoustics and Aeroelasticity of Turbomachines and Propellers, pp. 415-432, Springer Verlag

Dowell, E.H., Curtiss, H.C., Scanlan, R.H., and Sisto, F., 1978, " A modern course in aeroelasticity," Textbook, Sijthoff and Nordhoff, The Netherlands

Ducharme, E.H., Crawley, E.F., 1987, "Velocity Scaled Aeroelastic Testing of an Unducted Fan," GTL Report No. 191

Ekaterinaris, J.A., Platzer, M.F., 1997, "Computational Prediction of the Airfoil Dynamic Stall," Prog. Aerospace Sci. Vol. 33, pp. 759-846

Ekaterinaris, J.A., Platzer, M.F., 1996, " Numerical Investigation of Stall Flutter," Journal of Turbomachinery, Vol. 118, pp 197-203

Ekaterinaris, J.A., Chandrasekhara, M.S., Platzer, M.F., 1995, "Analysis of Low Reynolds Number Airfoil Flows," Journal of Aircraft, Vol. 32, No. 3, pp. 625-630

Ekaterinaris, J.A., Cricelli, A.S. and Platzer, M.F., 1994, "A Zonal Method for Unsteady Viscous Compressible Airfoil Flows," Journal of Fluids and Structures, Vol. 8, pp. 107-123

Gostelow, J.P., Melwani, N., and Walker, G.J., 1996, "Effects of a Streamwise Pressure Gradient on Turbulent Spot Development," ASME Journal of Turbomachinery, Vol. 118, pp.737-747

Grohsmeyer, S.P., Ekaterinaris, J.A. and Platzer, M.F., 1991, "Numerical Investigation of the Effect of Leading Edge Geometry on Dynamic Stall of Airfoils," AIAA 22nd Fluid Dynamics, Plasma Dynamics Lasers Conference, AIAA Paper No. 91-1798

McCroskey, W.J, McAlister, K.W., Carr, L.W., Pucci, S.L., 1982, "An Experimental Study of Dynamic Stall on Advanced Airfoil Sections," NASA Technical Memorandum 84245, Volume 1, 2 and 3, USAAVRADCOM TR-82-A-8

Rai, M.M. and Chakravarthy, S.R., 1988, "An Implicit Form of the Osher Upwind Scheme," AIAA Journal, Vol. 24, No. 5, May, pp. 735-743.

Sanz, W. and Platzer, M.F., 1998, "On the Navier-Stokes Calculation of Separation Bubbles With a New Transition Model," Journal of Turbomachinery, Vol. 120, pp. 36-42

Schewe, G. and Deyhle, H., 1996, "Experiments on Transonic Flutter of a Two-Dimensional Supercritical Wing with Emphasis on the Non-Linear-Effect," Proceedings of the Royal Aeronautical Society Conference on Unsteady Aerodynamics, London

Sisto, F., 1987, AGARD Manual on Aeroelasticity in Axial-Flow Turbomachines, AGARDograph No. 298, Vol. 1, Unsteady Turbomachinery Aerodynamics, Chap. 7, Stall Flutter, AGARD

Steger, J.L. and Warming, R.F., 1981, "Flux Vector Splitting of the Inviscid Gas Dynamic Equations with Applications to Finite-Difference Methods," Journal of Computational Physics, Vol. 40, pp. 263-293.

Teng, N.H., 1987, "The Development of a Computer Code for the Numerical Solution of Unsteady, Inviscid and Incompressible Flow over an Airfoil," Master's thesis, Naval Postgraduate School, Monterey, CA

Van Dyken, R.D., Ekaterinaris, J.A., 1996, "Analysis of Compressible Light Dynamic Stall Flow at Transitional Reynolds Numbers," AIAA Journal, Vol. 34, No. 7, pp. 1420-1427